Novel kinetic modeling of thiabendazole removal by adsorption and photocatalysis on porous organic polymers: effect of pH and visible light intensity

Alireza Ranjbari[a,b], Kristof Demeestere[b], Francis Verpoort[a,c], Ki-Hyun Kim[d],*,

Philippe M. Heynderickx[a,b],*

[a] Center for Environmental and Energy Research (CEER), Ghent University Global Campus, 119-5 Songdomunhwa-Ro, Yeonsu-Gu, Incheon 406-840, South Korea;

[b] Department of Green Chemistry and Technology, Faculty of Bioscience Engineering, Ghent University, Coupure Links 653, B-9000 Ghent, Belgium;

[c] Laboratory of Organometallics, Catalysis and Ordered Materials, State Key Laboratory of Advanced Technology for Materials Synthesis and Processing, Wuhan University of Technology, Wuhan, China;

[d] Department of Civil and Environmental Engineering, Hanyang University, Seoul 04763, Republic of Korea;

* kkim61@hanyang.ac.kr (K.-H. Kim), Philippe.Heynderickx@Ghent.ac.kr (P. M. Heynderickx)

Abstract

Visible light mediated heterogeneous photocatalysis of the fungicide thiabendazole (TBZ; initial concentration of 50 μmol/L) has been investigated using amorphous porous organic polymers (POPs). For the first time, both reversible adsorption in the dark and photocatalytic degradation under light irradiation are simultaneously monitored and kinetically modeled via coupled continuity equations for TBZ in both liquid phase and on the catalyst surface during a sequence of dark/light periods. The final model takes into account the effect of light intensity (28-120 W/m^2) and pH (3-9) on the adsorption and photocatalytic degradation processes. It is found that light intensity maintains a linear relation with both the degradation rate in the solution and on the catalyst surface, while it does not significantly affect the adsorption/desorption rates. The effect of pH was investigated in relation to the speciation of TBZ and its impact on adsorption/desorption and degradation coefficients. It is shown that the different TBZ species have distinct adsorption and desorption coefficients with their charge conditions. Furthermore, changes in pH have a significant effect on the overall removal by adsorption (highest at pH 6.8) or actual degradation (highest at pH 4.4).

The proposed model was satisfactory to describe the experimental data with a root-mean-square deviation (RMSD) of 1.88 μmol/L, corresponding to deviations below 4%. In addition, photocatalytic experiments under natural sunlight with a variable visible light intensity of 10 to 125 W/m^2 and reusability of the photocatalyst was successfully validated by the proposed model. Furthermore, the calculated quantum yield for the used POP mounts up to 2.8×10^{-6} molecules/photon with the space time yield reaches 1.5×10^{-6} molecules/(photon mg$_{cat}$), which is an order of magnitude higher than earlier reported values.

Keywords: Kinetic modeling, photocatalysis, porous organic polymers, visible light

1. Introduction

Heterogeneous photocatalytic degradation of organic compounds in liquid or gas phase is one of the most promising green technologies [1-5]. For the past half-century, a huge variety of semiconductor materials have been investigated as a photocatalyst to remove hazardous compounds [6, 7]. In spite of significant progress of the field, the advances of metal oxides or metal complexes has been confronted with some challenges such as a huge bandgap between valence and conduction band for visible light excitation, metal leaching, high price, and chemical instability [8-10]. Therefore, to help resolve such disadvantages, a new class of materials named porous organic polymers (POPs) has been developed for versatile applications such as photocatalyst, adsorbent, storage material, versatile reaction catalyst, and solid catalytic support [11, 12]. These novel polymers are tailored π-conjugated organic networks with nanoporous three-dimensional characteristics, providing a high surface area (200 to 1000 $m^2\,g^{-1}$) and great thermal/chemical stability [13, 14].

In this research, thiabendazole (TBZ) was used as a model compound for photocatalytic degradation. It is widely used in agriculture as a fungicide for crops, e.g., tomatoes, tobacco, sugar cane, rice, and fruits. In addition to crops, TBZ has also been applied in the treatment of hepatic diseases in goats and sheep. Because of extensive usage, its residues are found in agricultural run-off and in wastewater of food processing industries [15-18]. Not only because of its bio-activity and persistence [19], it can exert harmful effects on the aquatic environment. Further, it was also reported to be carcinogenic for humans in sufficiently high doses to interfere with the thyroid hormone balance [20, 21].

Kinetic modeling is one of the major approaches to assess the mechanism of photocatalytic degradation process. The Langmuir-Hinshelwood equation is the most commonly used for modeling to date [22-26]. If the concentration of model compound is sufficiently low, the Langmuir-Hinshelwood

equation can be simplified into an apparent first-order model [27-31]. Van Doorslaer et al. investigated the relation between adsorption and degradation rate [32]. A model was also proposed by considering the effect of intermediate compounds formed via photocatalytic degradation of dichlorophenol by TiO_2 [33]. Another kinetic study was performed by Rasoulifard et al. in visible light induced CdS nanocomposite by taking into account the adsorption and degradation on photocatalyst surface [34]. Other kinetic models have been proposed based on intrinsic element reactions [35], or the agglomerate diameter of the nano-particle [36]. In most of the reported studies, the compound degradation is modeled after the solution reaches adsorption equilibrium with the photocatalyst in the dark [37-41], although this dark period is often not specified in the modelling. Further, as the photocatalytic degradation is initiated by light irradiation, the reactions between electron holes and adsorbed compounds on the catalyst surface are not considered separately from those between active radicals and dissolved compounds in the liquid phase [22, 42]. Consequently, it is not possible to distinguish between the different degradation steps in the liquid phase and on the catalyst surface in the given kinetic model and it makes it impossible to describe the effect of variable experimental conditions such as pH and light intensity.

A reliable and detailed knowledge of the reaction kinetics is required to guarantee an optimal reactor design, advanced process control strategies, and improvement in safety and economic aspects of the process [43]. Therefore, the aim of this research is to develop a novel integrated model that considers the following continuous processes for the first time: (i) the reversible adsorption-desorption process of TBZ in the dark until the solution reaches equilibrium and (ii) its subsequent photocatalytic degradation both in the liquid phase and on the catalyst surface. Porous organic polymers (POPs) are used as visible light photocatalyst. In the computation of the kinetic model, the effects of experimental conditions, e.g., the ratio of catalyst to TBZ concentrations, light intensity, and pH, are taken into account to provide valuable insights into these stepwise processes. Furthermore, the feasibility of model has also been validated by

considering the changes in the intensity of natural sunlight, e.g., during different hours of the day. Finally, the reusability of POPs for photocatalysis has also been investigated.

2. Materials and methods

2.1. Chemicals

TBZ is provided by Sigma-Aldrich (analytical standard). H_3PO_4, KH_2PO_4, K_2HPO_4, and KOH (provided by DAEJUNG, South Korea >99%) are used to adjust pH, using pure water (HPLC grade). The information covering the detailed procedures for the synthesis of porous organic polymers (POP1) used in this study has been provided along with their characterization results in our previous work [13]. The schematic synthesis procedure of the POPs, together with the FE-SEM, TEM, and BET surface analysis of the catalyst is shown in section S.1 of the Supplementary Information.

2.2. Photocatalytic process

Table 1 gives the conditions for all conducted experiments. Dispersion of photocatalyst is an essential preparation step in a photocatalytic process [44]. However, in order to prevent premature adsorption, the catalyst and the contaminant should not be in contact during the sonication time. To this aim, POPs were sonicated in 12.5 mL of deionized water in an ultrasonic bath (MUJIGAE model SD-D200H, 40 kHz frequency) for 1 hour, while the required amount of TBZ was dissolved in a separate 12.5 mL deionized water. The dispersed solution of POPs was mixed and stirred with the TBZ solution (total volume of 25 mL) in the dark phase for 90 minutes to reach the equilibrium. After the dark phase, the lamp was switched on to initiate the degradation under visible light. The reaction was performed in a 100 mL beaker, while a Xenon lamp of DY TECH Co, model DXP300 (170-410 W) was placed on top of the beaker at a distance of 10 cm from the suspension surface (see section S.2 and Figure S.4 in the Supplementary Information).

To neutralize the effect of temperature, the beaker was placed in a water bath at room temperature (25 ±1°C). Light produced by the Xe lamp was filtered by a UV-IR cut-off filter (486 MRC Schneider Kreuznach) to ensure the photocatalytic process to proceed under visible light irradiation (420-670 nm). A 200 µL sample was taken from the suspension after 0, 1, 5, 15, 30, 60, and 90 minutes in the dark and after 15, 30, 60, 90, 120, 180, 240, 300, 360, and 420 minutes under exposure to visible light. Samples were diluted to 2 mL to be separated instantly by a syringe driven 0.22 µm PES membrane (Biofil) filter. The whole process of dilution and filtration was performed in less than 20 seconds to minimize TBZ desorption due to a change in equilibrium conditions of the diluted sample. Liquid TBZ concentrations were measured by HPLC-PDA as described in Section 2.3. Calibration curve data are mentioned in section S.3 of the Supplementary Information.

Model validation experiments were performed under natural sunlight. To have a similar light condition as during the lab experiments, the same UV-IR filter was placed on top of the beaker and its walls were covered by aluminum foil to prevent any UV beams inside the beaker.

In order to investigate the reusability of the POPs, experiment 1 from Table 1 was repeated and the catalyst was separated from the solution by centrifugation for 30 minutes with 10,000 rpm and dried under vacuum for 12 hours. The separated catalysts were weighed before adding to the subsequent batch and used under the given experimental conditions.

A control experiment (entry 1 in Table 1) was performed under visible light irradiation without POPs for 6 hours. As there was no significant change in the TBZ concentration in liquid phase (below 2% of the initial concentration), it was concluded that no significant photolysis took place in the overall TBZ degradation.

2.3. Analytical methods and equipment

TBZ concentrations were measured by an HPLC (SHIMADZU LC 2030C), equipped with an ACE 3 AQ column (150 x 3 mm) using a PDA detector at a wavelength of 300 nm. The mobile phase (500 µL/min) was an isocratic (65/35) mixture of methanol and 20 mM aqueous ammonium acetate [15]. An injection volume of 50 µL was applied. The calibration curve of the HPLC analysis is shown in Figure S.5 in the Supplementary Information. The limit of detection (LOD) and limit of quantification (LOQ) are calculated as 66.5 µg/L (or 0.33 µmol/L) and 22.2 µg /L (or 1.10 µmol/L) respectively; see section S.3 in Supplementary Information. Note that all TBZ concentrations in this work are quantified above the LOQ.

The solar power meter TES 132 was used to measure the intensity of the natural sunlight inside the same beaker used for the solution, while the UV-IR cut-off filter was placed on top of the beaker. The sunlight simulator light intensity was measured at the same distance of 10 cm that the solution would be placed. Additional aeration (air flow rate of 6 L/min) is done by Resun LiquidAir-4000 air pump and dissolved oxygen was measured by a Hanna HI9146 DO meter. COD was analyzed by USEPA 410.4 method by Hanna HI93754A-25 reagent and HI83314 photometer.

2.4. Basic kinetic model

In order to gain a comprehensive understanding on the photocatalytic process of TBZ, its removal in the solution phase has been monitored by considering reversible adsorption as well as degradation at the same time. The continuity equations (CE) of the starting kinetic model, named as model 1, are given by Eqs. (1) and (2):

$$\frac{d\left(VC_{aq}\right)}{dt} = -V(k_1 C_{aq} C_* - k_2 C_{ad}) - V k_3 C_{aq} \cdot \xi \quad (1)$$

$$\frac{d\left(m_{cat} C_{ad}\right)}{dt} = V(k_1 C_{aq} C_* - k_2 C_{ad}) - m_{cat} k_4 C_{ad} \cdot \xi \quad (2)$$

$$C_* + m\,C_{ad} = C_{tot} \quad (3)$$

$$\begin{cases} \xi = 0 \quad, \quad t < t^* \\ \xi = 1 \quad, \quad t^* \le t \end{cases} \quad (4)$$

Eq. (1) considers the adsorption from the bulk liquid to the catalyst surface as well as the degradation via radicals in the bulk liquid phase, with parameters k_1 and k_2 representing the adsorption and desorption rate coefficients, respectively. k_3 represents the apparent volumetric degradation rate coefficient in the liquid phase that is caused by active radicals. Eq. (2) describes the CE for TBZ adsorbate, taking into account the reversible adsorption and degradation by electron holes on the catalyst surface, while the parameter k_4 represents the apparent volumetric degradation rate coefficient of adsorbed TBZ by electron holes on the catalyst surface. The derivation of Eqs. (1) and (2) is presented in section S.4 of the Supplementary Information. Eq. (4) defines the light condition: for the first 90 minutes (t^*), during which the experiment is performed in the dark phase; thereafter, the light source is switched on. In the absence of light, the removal of TBZ is only due to adsorption; and the second term of both Eqs. (1) and (2) is zero. By turning the light on, the degradation of TBZ starts in both CEs.

Eq. (3) shows the site balance between free (C_*) and occupied (C_{ad}) active sites. Parameter m describes the average number of active sites that are occupied by one TBZ adsorbate molecule. The surface area of TBZ is calculated to be 82.1 Å^2 [45], while the surface area of the POPs is reported as 400 $\text{m}^2\,\text{g}^{-1}$ [11] and

the amount of active sites is estimated as 1.24×10^{-3} mol g^{-1}[46]. Hence, the average area for each active site can be calculated as 54 Å^2. If m is equal to 1 (as commonly done), this would erroneously underestimate the possible TBZ surface coverage since a TBZ molecule is larger than the area of an active site (ratio 1.52).

Excel$^®$ software is used for the numerical integration of the CE with a time step of 1 minute and a GRG nonlinear solving method by using an in-house written code. Kinetic parameters (k_1 to k_4, m, and C_{tot}) were estimated by minimizing the residual sum of squares (RSSQ), defined by Eq. (5), with n the number of experiments as mentioned in Table 1 and N_j the number of samples taken at each time point in each experiment:

$$S = \sum_{i=1}^{n} \sum_{j=1}^{N_j} (C_{aq,i,j} - \hat{C}_{aq,i,j})^2 \quad \rightarrow \quad \min \quad (5)$$

3. Results and discussion

As summarized in Table 1, a total of 15 experiments were conducted to construct and validate the best fitting model for combined adsorption and photocatalytic degradation in a stepwise manner. The first set of four experiments (entries of 1 to 4 in Table 1) was performed with a variable ratio of photocatalyst (40 and 80 mg/L) to TBZ concentration (10 and 15 mg/L). These data were used to estimate the parameters of model 1.

In order to investigate the effect of a variable light intensity (LI; 4 conditions from 28 to 120 W/m^2) and pH (4 conditions from 3.3 to 9.0), six experiments (entries 5 to 10) were conducted. Model 2 expands

model 1 and it includes the effect of LI on the TBZ degradation rate. Model 3 is designed to include the effect of the solution's pH on the adsorption and degradation coefficients.

The fourth (hereafter called 'final') model is developed based on all previous modeling insights and it considers the effect of both a variable LI and pH. The results of models 1, 2, and 3 (dashed lines) are compared with the final model (continuous lines) in Figures 1, 2, and 3, respectively. In this work, temperature effect is not investigated as the reaction rate of a photocatalytic process does not have a significant relationship with the minor temperature changes [47, 48]. The maximum value of visible light intensity of the sunlight in the validation experiments is about 125 W/m^2 and this is in the range of the performed experiments to evaluate model 2.

3.1. POPs to TBZ concentration ratio

During adsorption in the dark phase, the TBZ liquid concentration at equilibrium is determined by the amount of catalyst, the initial compound's concentration, and the adsorption coefficient, K_{ad}, see Eq. (6). At this point, the rates of adsorption and desorption are equal [49, 50] and the equilibrium liquid concentration can be obtained as solution of Eq. (6), see Section S.5 of the Supplementary Information:

$$C_{eq}^2 + C_{eq}(\frac{1}{K_{ad}} + \frac{m_{cat}}{V}C_{tot} - C_0) - \frac{C_0}{K_{ad}} = 0 \quad (6)$$

By changing the ratio of catalyst to TBZ concentration (q), as given in experiments 1 to 4 in Table 1, values of parameters k_1, k_2, k_3, k_4, C_{tot} and m in Eq. (1) to (3) can be estimated with model 1 as described in section 2.4, see Table 2. Figure 1 shows the experimental data and the calculated data for different q values. As can be observed, the concentration of TBZ reaches equilibrium at the end of the dark period and by increasing q from 2.7 to 8.0, the percentage of removal by adsorption of TBZ on the catalyst

surface in the dark increases from 34% to 81%. Higher TBZ removal by adsorption can be explained by the availability of more active sites at higher catalyst concentrations [51].

3.2. Light intensity

To investigate the effect of light intensity (LI), four different LI in the range 28-120 W/m^2 are applied, see entries 1, 5, 6, and 7 in Table 1. The dots in Figure 2 represent the experimental data, showing comparable results (48±5% removal) after the first 90 minute adsorption in the dark phase. By increasing the LI from 28 W/m^2 to 120 W/m^2, the total removal of TBZ also increased from 71% to 95% during degradation under visible light. A higher LI increases the production of electron-hole pairs to induce subsequent increases in the degradation rate [23, 52].

In order to consider the effect of LI in the kinetic modeling, k_3 and k_4 parameters were considered as an individual variable ($k_{3,i}$ and $k_{4,i}$) for each LI in model 2, and Eqs. (1) and (2) were rewritten as Eqs. (7) and (8):

$$\frac{d\left(VC_{aq}\right)}{dt} = -V(k_1 C_{aq} C_* - k_2 C_{ad}) - V k_{3,i} C_{aq} \cdot \xi \quad (7)$$

$$\frac{d\left(m_{cat} C_{ad}\right)}{dt} = V(k_1 C_{aq} C_* - k_2 C_{ad}) - m_{cat} k_{4,i} C_{ad} \cdot \xi \quad (8)$$

The values of $k_{3,i}$ and $k_{4,i}$ were estimated for a LI of 28, 53, 85 and 120 W/m^2 by integration of Eqs. (7) and (8) for experiments 1-7 of Table 1. The estimated values of the parameters of model 2 are listed in Table 2. The lines in Figure 2 are plotted by the calculated concentrations of TBZ in the solution for different LIs. From Figure S.6 in the Supplementary Information, showing the estimated values for

parameters $k_{3,i}$ and $k_{4,i}$ versus LI, it can be concluded that linear relations, given in Eqs. (9) and (10), can be proposed to correlate the degradation coefficients with the experimental LI:

$$k_3 = a \cdot LI \quad (9)$$

$$k_4 = b \cdot LI \quad (10)$$

When Eqs. (9) and (10) are modelled with an intercept, the latter was shown to be statistically not different from zero. This observation corresponds to the fact that there is no degradation of TBZ without light supply (LI = 0), as there are no radicals formed [53]. The obtained values for a and b are $(3.45 \pm 0.55) \, 10^{-5}$ and $(1.16 \pm 0.31) \, 10^{-5}$ respectively.

3.3. Effect of pH

In order to investigate the effect of pH on the TBZ degradation, the experimental conditions are extended with different pH values, ranging from 3.3 to 9 (entry 3, 8, 9, and 10 in Table 1). Figure 3 shows the results of adsorption and degradation of TBZ at different initial pH conditions. By increasing the pH from 3.3 to 6.8, the adsorptive removal of TBZ in the dark increased from 52% to 81%. However, a further increase to pH 9 decreased the adsorption removal to about 60%. The findings of such distinctive pH effect on the performance may be accounted for by changes in TBZ speciation across varying pH conditions. Inspection of the molecular structure of TBZ in Figure 4 suggests that the free electron pair on the second N atom of the central ring can receive a proton at acidic pH to impart a positive charge to the TBZ molecule. Also, the hydrogen atom at the first nitrogen of the central ring can be released into the solution at basic conditions, giving it a negative charge.

TBZ is an aromatic compound with several π bonds all around. In the structure of POPs (Figure S.1), the carbonaceous polymers are connected by π bonds. Although the POPs surface is without any charge, the adsorption of all species of TBZ on its surface can happen by π-π interactions [54]. However, because of electrical repulsion between positive adsorbates in acidic conditions and negative adsorbates in basic conditions, the adsorption coefficient is expected to be higher in neutral conditions. For the same reason, desorption coefficients are lower in neutral pH conditions than those of positive and negatively charged TBZ adsorbates due to an electrostatic repulsion force [55]. This discussion can be confirmed by considering the value for m, representing the average number of active sites that are occupied by one TBZ adsorbate molecule, see Eq. (3). As can be observed in Table 2, the value is estimated to be 1.24. This means that each of the TBZ molecules will occupy more than 1 active site of the catalyst, so that they will be placed at a close distance to each other during adsorption. If the majority of them have the same positive or negative charge, the consequent repulsion force will suppress the adsorption of TBZ (i.e., lower adsorption coefficient and higher desorption coefficient). However, in the case of the majority of neutral species around neutral pH conditions, the TBZ molecules can be bound on the surface without this repulsion force.

In order to consider the effect of pH in the kinetic model, TBZ speciation and the corresponding value for $K_{a,1}$ and $K_{a,2}$ have been taken into account, see Eqs. (11) to (13):

$$\alpha_0 = \frac{[AH_2^+]}{[A_T]} = \frac{[H^+]}{[H^+]^2 + K_{a,1}[H^+] + K_{a,1}K_{a,2}} \quad (11)$$

$$\alpha_1 = \frac{[AH]}{[A_T]} = \frac{K_{a,1}[H^+]}{[H^+]^2 + K_{a,1}[H^+] + K_{a,1}K_{a,2}} \quad (12)$$

$$\alpha_2 = \frac{[A^-]}{[A_T]} = \frac{K_{a,1}K_{a,2}}{[H^+]^2 + K_{a,1}[H^+] + K_{a,1}K_{a,2}} \quad (13)$$

The refined model 3 considers positive, neutral and negative species of TBZ, and each specimen has individual adsorption and desorption rate coefficients. The latter are shown as $k_{1,i}$ and $k_{2,i}$ in Eqs. (14) and (15) with i = 0, 1 or 2, representing the positive, neutral, and negative species, respectively. However, because of the high reactivity of radicals in the solution and electron holes on the surface, k_3 and k_4 are considered equal for all TBZ species. Hence, Eqs. (1) and (2) are updated and new CE for each specimen α_i can be presented as Eqs. (14) and (15):

$$V\frac{dC_{i,aq}}{dt} = -V(k_{1,i}\alpha_i C_{aq} C_* - k_{2,i}C_{i,ad}) - k_3 C_{i,aq}v\xi \quad (14)$$

$$m_{cat}\frac{dC_{i,ad}}{dt} = +V(k_{1,i}\alpha_i C_{aq} C_* - k_{2,i}C_{i,ad}) - k_4 C_{i,ad}m_{cat}\xi \quad (15)$$

Based on Eqs. (14) and (15), the CE for the total TBZ liquid and adsorbate concentrations are given by Eqs. (16) to (18):

$$V\frac{dC_{aq}}{dt} = -V\sum_{i=0}^{2}(k_{1,i}\alpha_i C_{aq} C_* - k_{2,i}C_{i,ad}) - Vk_3 C_{aq}\xi \quad (16)$$

$$m_{cat}\frac{dC_{ad}}{dt} = +V\sum_{i=0}^{2}(k_{1,i}\alpha_i C_{aq} C_* - k_{2,i}C_{i,ad}) - m_{cat}k_4 C_{ad}\xi \quad (17)$$

$$C_* + m\sum_{i=0}^{2}C_{i,ad} = C_{tot} \quad (18)$$

Dashed lines in Figure 3 represent the kinetic model, obtained by integration of Eqs. (16) to (18) and minimization of the RSSQ, see Eq. (5), using the experimental data corresponding to entry (1-4) and (8-

10) in Table 1. In this model, each specimen of TBZ has a specific k_1 and k_2 parameter and individual k_3 and k_4 parameters are considered per pH value, see Table 2 (model 3). In order to evaluate the α_i values, two additional parameters $pK_{a,1}$ and $pK_{a,2}$ are estimated. By integration of Eqs. (16) to (18), $pK_{a,1}$ and $pK_{a,2}$ are estimated as 5.09 and 7.96, respectively. The only experimental pK_a reported for TBZ is about 4.7 [45, 56] which is fairly close to the one estimated by the model. As expected, at pH 6.8 where TBZ has the maximum neutral speciation, adsorption in the dark stage shows the highest removal efficiency, as observed in Figure 4. A significant drop has been observed at pH 9 and 4.8, where the negative and positive species of TBZ become the majority, respectively. The estimated parameters in Table 2 for model 3 indicate that the adsorption rate coefficient of the positive and negative species of TBZ ($k_{1,0}$ and $k_{1,2}$) are smaller than that of the neutral specimen ($k_{1,1}$). The desorption rate coefficient $k_{2,0}$ and $k_{2,2}$ are higher than $k_{2,1}$ which results into a higher removal by adsorption at pH 6.8.

Figure 5 shows the individually estimated k_3 and k_4 for each pH in model 3. As it can be observed, k_3 has a reverse relationship with k_4. Basic pH values correspond to higher k_3 values, while the acidic pH values yield higher k_4 values. In basic solutions where the hydroxyl anion concentration is high enough, they can react with the electron holes on the catalyst surface to produce hydroxyl radicals that can favorably degrade TBZ in the solution, see Eqs. (19) to (22). On the contrary, as shown in Eq. (23), the electron holes at acidic condition, i.e., at negligible hydroxyl ion concentration, react directly with TBZ to cause its degradation [57-59]. The schematic representation of reaction mechanism is shown in Figure S.7 of the Supplementary Information.

$$POP + h\nu \rightarrow e_{CB}^- + h_{VB}^+ \quad (19)$$

$$HO^- + h_{VB}^+ \rightarrow HO^\bullet \quad (20)$$

$$(H_2O \leftrightarrow H^+ + HO^-) + h_{VB}^+ \rightarrow HO^\bullet + H^+ \qquad (21)$$

$$TBZ_{aq} + HO_{aq}^\bullet \rightarrow products \qquad (22)$$

$$TBZ_{ad} + h_{VB}^+ \rightarrow products \qquad (23)$$
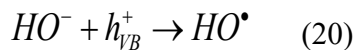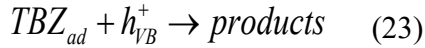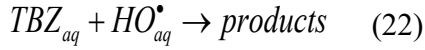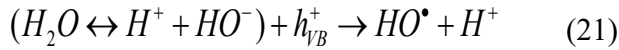
The dashed lines in Figure 5 show that estimated values for k_3 and k_4 can be considered to follow a hyperbolic function of pH, with the equations shown in section S.6 in the Supplementary Information. As a hyperbolic function, k_3 and k_4 cannot have negative values (they approach zero as their minimum). The maximal values for k_3 and k_4 are 4.4×10^{-3} min^{-1} at high basic pH values and 6.9×10^{-3} min^{-1} at low acidic pH values, respectively.

The combined effect of light intensity and pH on parameters k_3 and k_4, as given in Eqs. (9) and (10) and Figure 5 respectively, is represented via Eqs. (24) and (25):

$$k_3 = \frac{ae^{pH}}{1 + be^{pH}} \cdot LI \qquad (24)$$

$$k_4 = \frac{c}{1 + de^{pH}} \cdot LI \qquad (25)$$

All experiments, with corresponding conditions mentioned in entry (1-10) in Table 1, can be modeled by integration of CE (16) to (18), where the values of k_3 and k_4 are obtained by Eqs. (24) and (25). All continuous lines in Figures 1, 2, and 3 are calculated by the final model, i.e., all previous modeling insights with respect to the LI and pH are combined into one model. In this final model, by having fewer parameters than in model 3, a wider range of different conditions can be modeled with an error of less than 2% on the calculated removal efficiency.

In addition, the refinement of model 1 to become the final model is statistically investigated by (1) the evaluation of the F test for comparing nested models, as model 1 can be considered to be a simpler form of the final model [60] and (2) the RMSD value; see section S.8 of the Supplementary Information. The calculated F value (338.4) is higher than the tabulated F value (1.59), which confirms the statistical significance of the final model over the basic model 1. Also, it is shown that the RMSD value for the TBZ liquid concentration, obtained with the final model, is the lowest among all applied models (1.88 μmol/L corresponds to less than 4% of the initial TBZ concentration). Furthermore, the statistical adequacy of the final model is investigated by using the of lack-of-fit sum of squares [61]. For the final model, the pure error sum of squares is calculated as $3.31 \ 10^{-10}$ with 157 degrees of freedom, as described in section S.8 of the Supplementary Information. The lack-of-fit sum of squares of the final model is calculated as $3.65 \ 10^{-10}$ with 145 degrees of freedom to yield $F_c = 1.19$, see Eq. (S-26) in Supplementary Information. The tabulated F value with the corresponding degrees of freedom and $\alpha = 0.05$ is given as 1.31, which is higher than F_c and this result confirms the statistical adequacy of the final model.

The final model gives the opportunity to describe the photocatalytic degradation process with a variable pH and/or light intensity. For instance, for some degradation experiments, a pH drop of around 0.5 was observed during the degradation under visible light. In contrast, no significant pH drop was recorded during adsorption in the dark period. This can be explained by the presence of sulfur atoms in the TBZ structure and its presence in corresponding degradation products. In addition, as described in Eq. (21), in the process of hydroxyl radical production, some H^+ can be released into the solution to cause a slight drop in pH. The final model was used to consider this minor change in pH of the liquid solution with an increased accuracy. Practically, the experimental change in H^+ concentration was considered to be proportional to the degradation rate and a variable pH was implemented for every single minute of the

experiments. In conclusion, the final model is integrated by Eqs. (16) to (18), while individual pH and its corresponding α values were used for the calculation of k_3 and k_4 using Eqs. (24) and (25), respectively.

Table 2 shows the parameter estimates for the final model. In order to assess the adsorption parameters, the equilibrium coefficient for the TBZ species is calculated using the individual adsorption and desorption coefficients. For the positive, neutral, and negative TBZ species, the values are calculated as $2.14 \ 10^{+4}$, $5.36 \ 10^{+5}$, and $2.23 \ 10^{+4}$ L mol^{-1}, respectively. These values are in line with the experimental observations in Figure 4, where the neutral TBZ specimen shows the highest adsorption (at neutral pH condition). Compared to results for methylene blue (also containing 3 rings with sulphur and nitrogen atoms), values ranging from $4.70 \ 10^{+3}$ L mol^{-1} to $2.69 \ 10^{+5}$ L mol^{-1} were reported in the literature [27, 62-64]. It can be concluded that the values, obtained in this work, are within the same range. Note that the calculated equilibrium coefficient for models 1 and 2 is identically $4.62 \ 10^{+5}$ L mol^{-1}, which falls between the values for the different species. This is explained by the fact that these models did not take into account the effect of pH and, as a consequence, all TBZ species was considered to be neutral.

According to Eqs. (24) and (25), the values for k_3 range from $1.65 \ 10^{-4}$ min^{-1} (pH = 3, LI = 28 W/m^2) to $4.69 \ 10^{-3}$ min^{-1} (pH = 9, LI = 120 W/m^2). The values of k_4 vary from $3.12 \ 10^{-5}$ min^{-1} (pH = 9, LI = 28 W/m^2) to $6.82 \ 10^{-3}$ min^{-1} (pH = 3, LI = 120 W/m^2). This is in line with previously reported apparent kinetic parameters for methylene blue, ranging from $2.72 \ 10^{-3}$ min^{-1} to $5.86 \ 10^{-2}$ min^{-1} [63, 65-68]. Note that these parameters were obtained by using an apparent first order reaction. In this case, one reaction coefficient can be held responsible for the adsorption (accounting for apparent removal) as well as the degradation (by radicals in the liquid and by holes on the catalyst surface), which coincides with the given slightly higher value.

In this work, a value for the concentration of active sites is obtained as $8.73 \ 10^{-4}$ mol g^{-1}. Typical values for this parameter are around 10^{-3} mol g^{-1} in line with the literature reports [69, 70].

The proposed model clearly shows that the adsorption equilibrium of TBZ with the catalyst is established by starting each experiment in the dark period. The adsorption has initially a higher rate than the desorption, but eventually the solution reaches equilibrium (no net adsorption/desorption). By the start of the light period, the equilibrium will shift in one direction, depending on the pH of the solution and its effect on the degradation rates in the solution and on the catalyst surface.

Lastly, the applicability of the proposed model and the necessary conditions for its application in other photocatalytic degradation studies are discussed in section S.13 of the Supplementary Information and the mineralization of TBZ during the photocatalytic degradation has been investigated in section S.14.

3.4. Dissolved oxygen

The experiments, with conditions corresponding to entry 1 to 10 in Table 1, were performed without additional aeration. In order to investigate the effect of dissolved oxygen and the possible production of superoxide radicals as a result of the reaction between oxygen and electrons, additional experiments (entry 11-13 in Table 1 at pH 3.3, 6.8, and 9.0) were performed with specific aeration.

It is proven that the main free radicals that affect photocatalytic degradation are hydroxyl radicals [71]. The latter can be produced by direct reaction of hydroxyl anions and electron holes, as described in Eqs. (20) and (21). Another possibility for the hydroxyl radical formation is the reaction of dissolved oxygen and electron holes, producing hydrogen peroxide that further decomposes as shown in Eqs. (26) to (29) [27, 72-74]:

$$O_2 + e^-_{CB} \rightarrow O_2^{\bullet -} \qquad (26)$$

$$O_2^{\bullet -} + H^+ \rightarrow HO_2^{\bullet} \qquad (27)$$

$$2HO_2^{\bullet} \rightarrow H_2O_2 + O_2 \qquad (28)$$

$$H_2O_2 + e^- \rightarrow HO^- + HO^{\bullet} \qquad (29)$$
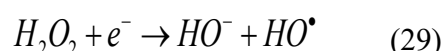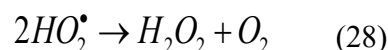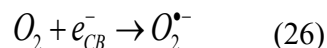
As it is shown in Figure S.8 in the Supplementary Information, no significant difference was observed in the results between the experiments with and without aeration. It is reported that oxygen transfer into the solution can take place through the interaction between the liquid and air by continuous stirring in an open reactor [75]. The oxygen transfer rate into the reactor during the experiment is calculated, as previously reported by Ollis et al. [76], see section S.9 in the Supplementary Information. Since the reactor volume is 25 ml and the liquid depth is less than 2 cm, the solution for the experiments without aeration can be considered to be saturated with oxygen. This assumption was checked and confirmed by the experimental measurement of the dissolved oxygen concentration before and after the reaction, which was about 8 mg/l at room temperature.

In conclusion, the k_3 parameter already reflects the effect of major active radicals (hydroxyl and superoxide radicals) in the presence of visible light source, as shown in Eq. (30):

$$k_3 = k_{3,1} C_{HO^{\bullet}} + k_{3,2} C_{O_2^{\bullet -}} \qquad (30)$$

It should be noted that k_3 in Eq. (9) or (24) is dependent on the light intensity as no active radicals can be produced at LI = 0.

3.5. Model validation under natural sunlight

Since the sunlight intensity continuously changes during the day, it is very important to properly simulate the complicated conditions for a continuous photocatalytic degradation process, especially under varying conditions of pH and LI. For this purpose, three experiments (entry 14 in Table 1) are performed at an initial pH of 4.8, 6.8, and 9.0 under real and variable sunlight conditions (LI between 10 and 125 W/m^2). The experiments were performed in the dark for the first 90 minutes, so that the solution reaches equilibrium. The dots in Figure 6 show the experimental data, which indicate that the highest removal by adsorption (47%) is obtained at pH 6.8. Since the experiments were performed on different days and different hours of the day, the degradation of TBZ in each experiment started under different irradiation conditions. Hence, the changes in light intensity for each experiment were modeled by a polynomial curve, which was plugged into in Eqs. (24) and (25) to estimate k_3 and k_4, respectively at every 1 minute time span (see section S.10 and Figure S.9 in the Supplementary Information). The continuous lines in Figure 6a correspond to the calculated data by the final model using Eqs. (16) to (18) and their corresponding k_3 and k_4 calculated by Eqs. (24) and (25). Figure 6b shows the parity plot of the experimental and calculated data, which shows a high accuracy in the final model's results.

3.6. Simulation of TBZ removal

In the final model, Eqs. (16) to (18) are used to simulate the adsorbed TBZ on the catalyst surface in order to offer insight into the contribution of different variables in specific adsorption and degradation processes in the overall TBZ removal. As an outcome of Eq. (17), Figure 7a illustrates the total moles of TBZ adsorbed on the catalyst surface. The highest adsorption of TBZ is achieved at pH 6.8, in agreement with what has been described in Section 3.3. As can be observed, after 20 hours, still a considerable

amount of TBZ remains on the catalyst surface in pH 6.8 and 9.0, while almost all adsorbed TBZ molecules are degraded at pH 3.3 and 4.8. Such relationship is also supported by the higher desorption coefficients on the catalyst surface (k_4) at lower pH values.

To compare the net degradation of TBZ at different pH values, the total amount of remaining TBZ (T) in the system was calculated on every time step by Eq. (31), where C_{aq} and C_{ad} were obtained via integration of Eqs. (16) and (17), respectively:

$$T = VC_{aq} + m_{cat}C_{ad} \quad (31)$$

Figure 7b shows the total moles of TBZ, i.e., the sum of both TBZ in solution and on the catalyst surface, as a function of time and at different pH. During the adsorption in the dark, the total moles of TBZ in the process are constant. At the start of photocatalytic degradation, the curves at acidic pH values 3.3 and 4.8 show comparable total degradation, which is higher than the degradation at pH values 6.8 and 9. On the other hand, Figure 3 shows that the experimental and calculated concentrations of TBZ in solution are lower at pHs 6.8 and 9, compared to the acidic pHs of 4.8 and 3.3. The reason for these observations is that the highest removal by adsorption (~ 81%) is reached at pH 6.8, and because of a low k_4 value at this pH, the adsorbed TBZ on the catalyst surface slowly reacts with electron holes. As a result, even after 20 hours a large portion of adsorbed TBZ remains unreacted.

To find the optimum pH for total TBZ removal, both degradation in the solution and on the catalyst surface should be taken into account. Hence, the total degradation rate (P, in mol min^{-1}) of TBZ can be written as Eq. (32):

$$P = Vk_3C_{aq} + m_{cat}k_4C_{ad} \quad (32)$$

Figure 8a shows the values of P, simulated for every 1 minute time increment of experiments with pH ranging between 3 and 11. Similar to the discussion in Figure 7b, at the beginning of the photocatalytic degradation (t < 7 hrs), the maximum degradation rates are found under acidic pH between 3 and 5, while the minimum values of P occur at around neutral pH. With the passage of time, the sum of TBZ concentration, i.e., in the solution plus on the catalyst surface, will change. After 10 hours of degradation under visible light irradiation, the interaction of the TBZ in the solution and on the catalyst surface with degradation coefficients k_3 and k_4, causes the maximum P values to occur at neutral pH values.

Figure 8b plots X, which is defined by the ratio of the TBZ degradation rate in the liquid phase to the total degradation rate (P), see Eq. (33), as a function of reaction time for pH values ranging from 3 to 11:

$$X = \frac{Vk_3 C_{aq}}{Vk_3 C_{aq} + m_{cat} k_4 C_{ad}} \qquad (33)$$

At pH values higher than 9, where higher values of k_3 are expected, the majority of degradation takes place by reactions in solution phase during the whole experiment. On the other hand, at the acidic pHs, X displays a low value due to a higher value for k_4. At the beginning of the degradation process (t < 1 hr), most of the degradation take place in the solution for neutral pH values. By the decrease of TBZ concentration in solution and the consequent drop in degradation rate in the liquid, X shows lower values as the reaction progressed.

In order to describe the specific interplay between adsorption and degradation, the ratio of adsorption rate versus total degradation rate (P) is defined by Eq. (34):

$$Z = \frac{V \sum_{i=0}^{2} (k_{1,i} \alpha_i C_{aq} C_* - k_{2,i} C_{i,ad})}{Vk_3 C_{aq} + m_{cat} k_4 C_{ad}} \qquad (34)$$

Note that the solution has reached equilibrium in the first 90 minutes of the dark phase and the catalyst has no additional capacity to host more TBZ molecules. However, it is observed that the Z ratio still has a large value at acidic pH (see Figure 8c). This is because k_4 is greater than k_3 at these acidic pH values and the degradation proceeds faster on the catalyst surface than in the solution. Consequently, the concentration of TBZ adsorbate molecules is decreasing faster, compared to the liquid TBZ concentration decrease. This causes a shift in the adsorption equilibrium and the overall TBZ net adsorption rate increases.

On the other hand, at pH higher than 7, the degradation rate in the solution is higher than on the catalyst surface, which is in line with a higher value of k_3. As a result, the decrease of TBZ concentration in the solution is faster and, in order to maintain the equilibrium, negative values for Z are found at basic pH conditions, as some TBZ should be desorbed from the catalyst surface (Figure 8c). At pH 9 the maximum negative value for Z is observed, whereas a neutral pH shows less negative values. The reason is that most of the TBZ molecules at this pH are in neutral speciation (AH) which has a higher adsorption coefficient and a lower desorption coefficient than other species (see Table 2).

When the adsorption has a significant contribution to the contaminant's removal from the solution, it is vital to consider both adsorption and degradation separately in the overall TBZ removal. If the goal for treatment is rapid water purification, a neutral pH can be considered as the optimum pH. However, if the goal is being set as total TBZ removal by photocatalytic degradation, both reactions in the solution and on the catalyst surface should be taken into account. As can be observed in Figure 8a, the highest degradation rate of P is found in the beginning of photocatalytic degradation at pH 4.4, which is the optimum pH for total TBZ degradation.

3.7. Quantum yield

The energy consumption of a photocatalyst plays an important role in the selection of a photocatalytic system. The quantum yield (QY) can be defined as the ratio of the total amount of TBZ molecules degraded per second to the total number of photons entering the solution per second [77]. Details of its calculation can be found in section S.11 in the Supplementary Information. In Figure S.10a, QY values are found to increase with changes in LI from 28 to 85 W/m^2. A further increase in LI decreases the QY and, hence, this is considered not to be energy efficient. Figure S.10b indicates that pH 4.8 has the highest QY due to the highest TBZ degradation. The experiments at neutral and basic pH values have a somewhat lower QY values, since the removal for these pH values is mostly by adsorption rather than by degradation.

The calculated QY for the POP ranges from 1.2×10^{-6} to 2.8×10^{-6} molecules/photon. The used catalyst shows a good performance when the QY values, computed in this work, are compared with those reported from different photocatalysts (in methylene blue degradation), ranging from 6.7×10^{-8} to 3.8×10^{-6} molecules/photon [77].

To account for the efficiency per net mass of photocatalyst in the QY calculations, the space time yield (SY) can be computed in terms of the ratio between the QY and the used catalyst mass. On average, the SY for used POP is about 1.5×10^{-6} molecules/photon mg$_{cat}$. This value also supports the superiority of the POP system over others, reported to have SY values in the range of 2.8×10^{-10} to 1.0×10^{-7} molecules/photon mg$_{cat}$ [77]. This indicates an excellent (one order of magnitude increase) performance of the POP catalysts, when SY is taken as comparison basis. Major reason is that (on average) ~10 times less catalyst is used in this work, compared to the other aforementioned studies, to achieve a similar level of catalytic activity.

3.8. Reusability of POP photocatalyst

In order to investigate the reusability of the photocatalyst for TBZ degradation, 6 cycles of the process are simulated, and the calculated data are shown in Figure 9a. The conditions for the first run was set identically as experiment 1 in Table 1, i.e., 90 minutes of adsorption in the dark and 7 hours of degradation under visible light irradiation. Afterwards, another 7 hours of photodegradation is simulated under visible light over additional five cycles by maintaining the TBZ concentration to 5 mg/l to match the initial conditions for the photodegradation in the first run. The photocatalytic removal of TBZ from the solution for each simulated cycle is shown in Figure 9b. The percentage removal of TBZ is calculated by considering its liquid concentration before and after the light irradiation of each cycle.

Next to data simulation, laboratory experiments are performed to investigate the reusability of the photocatalyst at the same conditions as described for the simulations. Figure 9b shows the normalized experimental TBZ removal efficiency at each run by taking its aqueous concentration at the beginning and at the end of the degradation process. The first use of catalyst resulted in an experimental efficiency of 87%, which is almost the same as the simulated data. After 5 times of reuse, the experimental degradation efficiency decreased to 80%, while the simulated data still show an efficiency of about 90%. This reduction in experimental removal efficiency may reflect the loss of catalyst during the separation process after each run as it decreased from 1.0 to 0.9 mg after 5 cycles (a loss of about 10%). As the overall experimental degradation efficiency shows about 12% of reduction relative to the simulated data, the activity loss is suspected to be caused mainly by the loss of catalyst, rather than the decrease in the catalytic activity of the POP itself.

In order to consider the effect of pH on photocatalyst reuse, the same simulation is performed at the optimum pH of 4.4 for the total degradation of TBZ in liquid and on the catalyst surface. Figure S.12 in

the Supplementary Information illustrates the results of this simulation. Due to a lower adsorption in the dark phase for the first cycle, the degradation begins with a higher aqueous concentration of TBZ that results in a lower removal of about 90% under visible light irradiation. However, after a few cycles, the aqueous TBZ removal reaches its maximum of about 94% in each reuse cycle. This observation indicates a slight increase in the aqueous TBZ removal comparing to pH 6.8, while the adsorbed TBZ remaining on the catalyst surface at the end of each cycle is decreased from 0.45 μmol at pH 6.8 to 0.11 μmol at pH 4.4.

4. Conclusions

Porous organic polymers (POP) have shown great practicality as photocatalyst for thiabendazole (TBZ) degradation under visible light irradiation. This system was found to achieve a total of 96% removal of TBZ under the optimal conditions, e.g., after 90 minutes of adsorption in the dark and 7 hours of degradation under visible light. The optimum pH for adsorption is pH 6.8, while the optimum pH for the maximal photocatalytic degradation is 4.4. It was shown that natural sunlight could be used as a green source of energy for this process while POPs are reusable in new batches several times.

A new kinetic model is developed to address the various aspects of the target TBZ removal by considering the combined features of adsorption and photocatalytic degradation processes in a stepwise manner as follows: (1) the reversible adsorption-desorption reactions are simultaneously described with the degradation process, (2) TBZ concentrations are tracked separately in the liquid and on the catalyst surface, and (3) degradation of aqueous TBZ by radicals and of adsorbed TBZ by electron holes are individually taken into account.

Based on a systematic evaluation of all controlling factors that interact for the removal of TBZ adsorption/desorption, catalytic reaction coefficients are determined as a function of key variables including light intensity and pH of the solution. Furthermore, it was shown that at higher pH values, the degradation is mostly by active radicals in the liquid, while it is by the electron holes on the catalyst surface at lower pH values. In addition, the estimated pK_a values for TBZ are found to be accurate and, as such, this approach can be recommended as an indirect method for the calculation and prediction of pK_a values for other compounds.

Acknowledgements

List of symbols

Roman symbols

C	Concentration of total species of thiabendazole	mol L^{-1}
C$_*$	Concentration of available active sites on catalyst surface	mol g^{-1}
C$_{tot}$	Concentration of total active sites on catalyst surface	mol g^{-1}

F_c	Test statistic for lack-of-fit model evaluation	-
k_1	Adsorption rate coefficient	g mol^{-1} min^{-1}
k_2	Desorption rate coefficient	g L^{-1} min^{-1}
k_3	Degradation rate coefficient by active radicals in solution	min^{-1}
k_4	Degradation rate coefficient by electron holes at catalyst surface	min^{-1}
K_{ad}	Adsorption coefficient	L mol^{-1}
K_a	Acid dissociation constant	mol L^{-1}
m	Occupied active sites to adsorbed thiabendazole molecules ratio	mol mol^{-1}
m_{cat}	Catalyst mass	g
n	Number of each experiment	-
N_j	Number of samples at different retention times in an experiment	-
q	Ratio of POPs (mg/L) over thiabendazole (mg/L)	-
V	Volume of the solution	L
S	Residual sum of squares	mol^2 L^{-2}
P	Total photocatalytic degradation rate	mol min^{-1}
X	Ratio of aqueous degradation rate over total degradation rate	-
Z	Ratio of total adsorption rate over total degradation rate	-

Greek symbols

α_i Partition ratio of species i   mol mol^{-1}

ξ Light switch (= 0 for the dark zone; = 1 for the light zone, see Eq. (4))   -

Subscripts

ad   Adsorbed

aq   Aqueous

i   Specimen of thiabendazole

exp   Experimental data

^   Calculated value

Abbreviations and acronyms

A^- Negative thiabendazole specimen

AH   Neutral thiabendazole molecule

AH_2^+ Positive thiabendazole specimen

A_T Total thiabendazole specimen

CE   Continuity equation

COD   Chemical oxygen demand

LI   Light intensity   W m^{-2}

LOD   Limit of detection   mg L^{-1} or mol L^{-1}

LOQ   Limit of quantification $mg\ L^{-1}$ or $mol\ L^{-1}$

POP   Porous organic polymer

RMSD Root-mean-square deviation

RSSQ Residual sum of squares $mol^2\ L^{-2}$

QY   Quantum yield $molecules\ photon^{-1}$

SY   Space time yield $molecules\ photon^{-1}\ mg_{cat}^{-1}$

TBZ   Thiabendazole

References

[1] X. Wang, M. Sun, M. Murugananthan, Y. Zhang, L. Zhang, Electrochemically self-doped WO_3/TiO_2 nanotubes for photocatalytic degradation of volatile organic compounds, Appl. Catal., B, 260 (2020) 118205.

[2] K. Ye, Y. Li, H. Yang, M. Li, Y. Huang, S. Zhang, H. Ji, An ultrathin carbon layer activated CeO_2 heterojunction nanorods for photocatalytic degradation of organic pollutants, Appl. Catal., B, 259 (2019) 118085.

[3] A. Ranjbari, N. Mokhtarani, Post treatment of composting leachate using ZnO nanoparticles immobilized on moving media, Appl. Catal., B, 220 (2018) 211-221.

[4] S. Deepracha, A. Ayral, M. Ogawa, Acceleration of the photocatalytic degradation of organics by in-situ removal of the products of degradation, Appl. Catal., B, 284 (2021) 119705.

[5] Z. Wang, L. Jiang, K. Wang, Y. Li, G. Zhang, Novel $AgI/BiSbO_4$ heterojunction for efficient photocatalytic degradation of organic pollutants under visible light: Interfacial electron transfer pathway, DFT calculation and degradation mechanism study, J. Hazard. Mater., 410 (2021) 124948.

[6] A. Di Paola, E. García-López, G. Marcì, L. Palmisano, A survey of photocatalytic materials for environmental remediation, J. Hazard. Mater., 211-212 (2012) 3-29.

[7] M.I. Litter, W. Choi, D.D. Dionysiou, P. Falaras, A. Hiskia, G. Li Puma, T. Pradeep, J. Zhao, Nanotechnologies for the treatment of water, air and soil, J. Hazard. Mater., 211-212 (2012) 1-2.

[8] Y. Qu, X. Duan, Progress, challenge and perspective of heterogeneous photocatalysts, Chem. Soc. Rev., 42 (2013) 2568-2580.

[9] H. Tong, S. Ouyang, Y. Bi, N. Umezawa, M. Oshikiri, J. Ye, Nano-photocatalytic materials: possibilities and challenges, Adv. Mater., 24 (2012) 229-251.

[10] J. Luo, X. Zhang, J. Zhang, Carbazolic porous organic framework as an efficient, metal-free visible-light photocatalyst for organic synthesis, ACS Catal., 5 (2015) 2250-2254.

[11] J. Chakraborty, I. Nath, S. Song, S. Mohamed, A. Khan, P.M. Heynderickx, F. Verpoort, Porous organic polymer composites as surging catalysts for visible-light-driven chemical transformations and pollutant degradation, J. Photochem. Photobiol., C, 41 (2019) 100319.

[12] T. Zhang, G. Xing, W. Chen, L. Chen, Porous organic polymers: a promising platform for efficient photocatalysis, Mater. Chem. Front., 4 (2020) 332-353.

[13] I. Nath, J. Chakraborty, P.M. Heynderickx, F. Verpoort, Engineered synthesis of hierarchical porous organic polymers for visible light and natural sunlight induced rapid degradation of azo, thiazine and fluorescein based dyes in a unique mechanistic pathway, Appl. Catal., B, 227 (2018) 102-113.

[14] J. Chakraborty, I. Nath, C. Jabbour, N. Aljammal, S. Song, C.-M. Kao, P.M. Heynderickx, F. Verpoort, Novel rapid room temperature synthesis of conjugated microporous polymer for metal-free photocatalytic degradation of fluoroquinolones, J. Hazard. Mater., (2020) 122928.

[15] P. Calza, S. Baudino, R. Aigotti, C. Baiocchi, E. Pelizzetti, Ion trap tandem mass spectrometric identification of thiabendazole phototransformation products on titanium dioxide, J. Chromatogr. A, 984 (2003) 59-66.

[16] R. Igual-Adell, C. Oltra-Alcaraz, E. Soler-Company, P. Sánchez-Sánchez, J. Matogo-Oyana, D. Rodríguez-Calabuig, Efficacy and safety of ivermectin and thiabendazole in the treatment of strongyloidiasis, Expert Opin. Pharmacother., 5 (2004) 2615-2619.

[17] R. Portugal, R. Schaffel, L. Almeida, N. Spector, M. Nucci, Thiabendazole for the prophylaxis of strongyloidiasis in immunosuppressed patients with hematological diseases: a randomized double-blind placebo-controlled study, Haematologica, 87 (2002) 663-664.

[18] A. Bernabeu, R. Vercher, L. Santos-Juanes, P. Simón, C. Lardín, M. Martínez, J. Vicente, R. González, C. Llosá, A. Arques, Solar photocatalysis as a tertiary treatment to remove emerging pollutants from wastewater treatment plant effluents, Catal. Today, 161 (2011) 235-240.

[19] C. Sirtori, A. Agüera, I. Carra, J.A.S. Pérez, Identification and monitoring of thiabendazole transformation products in water during Fenton degradation by LC-QTOF-MS, Anal. Bioanal.Chem., 406 (2014) 5323-5337.

[20] M. Jiménez, M. Ignacio Maldonado, E.M. Rodríguez, A. Hernández-Ramírez, E. Saggioro, I. Carra, J.A. Sanchez Perez, Supported TiO_2 solar photocatalysis at semi-pilot scale: degradation of pesticides found in citrus processing industry wastewater, reactivity and influence of photogenerated species, J. Chem. Technol. Biotechnol., 90 (2015) 149-157.

[21] S. Kumar, A. Kumar, A. Kumar, R. Balaji, V. Krishnan, Highly efficient visible light active 2D-2D nanocomposites of N-ZnO-g-C_3N_4 for photocatalytic degradation of diverse industrial pollutants, ChemistrySelect, 3 (2018) 1919-1932.

[22] I.K. Konstantinou, T.A. Albanis, TiO_2-assisted photocatalytic degradation of azo dyes in aqueous solution: kinetic and mechanistic investigations: a review, Appl. Catal., B, 49 (2004) 1-14.

[23] M.A. Behnajady, N. Modirshahla, R. Hamzavi, Kinetic study on photocatalytic degradation of C.I. Acid Yellow 23 by ZnO photocatalyst, J. Hazard. Mater., 133 (2006) 226-232.

[24] M. Malayeri, F. Haghighat, C.-S. Lee, Kinetic modeling of the photocatalytic degradation of methyl ethyl ketone in air for a continuous-flow reactor, Chem. Eng. J., 404 (2021) 126602.

[25] M. Malayeri, C.-S. Lee, J. Niu, J. Zhu, F. Haghighat, Kinetic modeling and reaction mechanism of toluene and by-products in photocatalytic oxidation reactor, Chem. Eng. J., 427 (2022) 131536.

[26] N. Riaz, M. Hassan, M. Siddique, Q. Mahmood, U. Farooq, R. Sarwar, M.S. Khan, Photocatalytic degradation and kinetic modeling of azo dye using bimetallic photocatalysts: effect of synthesis and operational parameters, Environ. Sci. Pollut. Res., 27 (2020) 2992-3006.

[27] A. Houas, H. Lachheb, M. Ksibi, E. Elaloui, C. Guillard, J.-M. Herrmann, Photocatalytic degradation pathway of methylene blue in water, Appl. Catal., B, 31 (2001) 145-157.

[28] I.K. Konstantinou, T.A. Albanis, Photocatalytic transformation of pesticides in aqueous titanium dioxide suspensions using artificial and solar light: intermediates and degradation pathways, Appl. Catal., B, 42 (2003) 319-335.

[29] F. Zhou, C. Yan, T. Liang, Q. Sun, H. Wang, Photocatalytic degradation of Orange G using sepiolite-TiO_2 nanocomposites: Optimization of physicochemical parameters and kinetics studies, Chem. Eng. Sci., 183 (2018) 231-239.

[30] C. Yang, W. Dong, G. Cui, Y. Zhao, X. Shi, X. Xia, B. Tang, W. Wang, Highly efficient photocatalytic degradation of methylene blue by P2ABSA-modified TiO_2 nanocomposite due to the photosensitization synergetic effect of TiO_2 and P2ABSA, RSC Adv., 7 (2017) 23699-23708.

[31] Y.-J. Lee, J.-K. Kang, S.-J. Park, C.-G. Lee, J.-K. Moon, P.J.J. Alvarez, Photocatalytic degradation of neonicotinoid insecticides using sulfate-doped Ag_3PO_4 with enhanced visible light activity, Chem. Eng. J., 402 (2020) 126183.

[32] X. Van Doorslaer, K. Demeestere, P.M. Heynderickx, H. Van Langenhove, J. Dewulf, UV-A and UV-C induced photolytic and photocatalytic degradation of aqueous ciprofloxacin and moxifloxacin: Reaction kinetics and role of adsorption, Appl. Catal., B, 101 (2011) 540-547.

[33] B. Bayarri, J. Giménez, D. Curcó, S. Esplugas, Photocatalytic degradation of 2,4-dichlorophenol by TiO_2/UV: Kinetics, actinometries and models, Catal. Today, 101 (2005) 227-236.

[34] M.H. Rasoulifard, M.S. Seyed Dorraji, A.R. Amani-Ghadim, N. Keshavarz-babaeinezhad, Visible-light photocatalytic activity of chitosan/polyaniline/CdS nanocomposite: Kinetic studies and artificial neural network modeling, Appl. Catal., A, 514 (2016) 60-70.

[35] A.R. Khataee, M. Fathinia, S. Aber, Kinetic study of photocatalytic decolorization of C.I. Basic Blue 3 solution on immobilized titanium dioxide nanoparticles, Chem. Eng. Res. Des., 89 (2011) 2110-2116.

[36] Q. Geng, J. Yang, L. Wang, A novel kinetic model to estimate the agglomerate diameter formed by nano-sized Titania in emulsion region of AFBPR, Chem. Eng. J., 360 (2019) 1477-1485.

[37] P. Pascariu, C. Cojocaru, N. Olaru, P. Samoila, A. Airinei, M. Ignat, L. Sacarescu, D. Timpu, Novel rare earth (RE-La, Er, Sm) metal doped ZnO photocatalysts for degradation of Congo-Red dye: Synthesis, characterization and kinetic studies, J. Environ. Manage., 239 (2019) 225-234.

[38] N. Omrani, A. Nezamzadeh-Ejhieh, A novel quadripartite Cu_2O-CdS-$BiVO_4$-WO_3 visible-light driven photocatalyst: Brief characterization and study the kinetic of the photodegradation and mineralization of sulfasalazine, J. Photochem. Photobiol., A, 400 (2020) 112726.

[39] N. Singh, M.S. Rana, R.K. Gupta, Modelling studies for photocatalytic degradation of organic dyes using TiO_2 nanofibers, Environ. Sci. Pollut. Res., 25 (2018) 20466-20472.

[40] M.F. Atitar, A. Bouziani, R. Dillert, M. El Azzouzi, D.W. Bahnemann, Photocatalytic degradation of the herbicide imazapyr: do the initial degradation rates correlate with the adsorption kinetics and isotherms?, Catal. Sci. Technol., 8 (2018) 985-995.

[41] M. Zulfiqar, S. Chowdhury, M.F.R. Samsudin, A.A. Siyal, A.A. Omar, T. Ahmad, S. Sufian, Effect of organic solvents on the growth of TiO_2 nanotubes: An insight into photocatalytic degradation and adsorption studies, J. Water Process Eng., 37 (2020) 101491.

[42] A. Bianco Prevot, C. Baiocchi, M.C. Brussino, E. Pramauro, P. Savarino, V. Augugliaro, G. Marci, L. Palmisano, Photocatalytic degradation of acid blue 80 in aqueous solutions containing TiO_2 suspensions, Environ. Sci. Technol., 35 (2001) 971-976.

[43] G. Ganzer, H. Freund, Kinetic Modeling of the Partial Oxidation of Propylene to Acrolein: A Systematic Procedure for Parameter Estimation Based on Non-isothermal Data, Ind. Eng. Chem. Res., 58 (2019) 1857-1874.

[44] J.C. Garcia, K. Takashima, Photocatalytic degradation of imazaquin in an aqueous suspension of titanium dioxide, J. Photochem. Photobiol., A, 155 (2003) 215-222.

[45] B. Lombardi, M. Baschini, R.M. Torres Sánchez, Optimization of parameters and adsorption mechanism of thiabendazole fungicide by a montmorillonite of North Patagonia, Argentina, Appl. Clay Sci., 24 (2003) 43-50.

[46] M.P. Heynderickx, J.W. Thybaut, H. Poelman, D. Poelman, G.B. Marin, Kinetic modeling of the total oxidation of propane over $CuO-CeO_2/\gamma-Al_2O_3$, Appl. Catal., B, 95 (2010) 26-38.

[47] R. Al-Rasheed, D.J. Cardin, Photocatalytic degradation of humic acid in saline waters. Part 1. Artificial seawater: influence of TiO_2, temperature, pH, and air-flow, Chemosphere, 51 (2003) 925-933.

[48] M.A. Fox, M.T. Dulay, Heterogeneous photocatalysis, Chem. Rev., 93 (1993) 341-357.

[49] S. Helali, E. Puzenat, N. Perol, M.-J. Safi, C. Guillard, Methylamine and dimethylamine photocatalytic degradation—Adsorption isotherms and kinetics, Appl. Catal., A, 402 (2011) 201-207.

[50] F. Zhang, J. Zhao, T. Shen, H. Hidaka, E. Pelizzetti, N. Serpone, TiO_2-assisted photodegradation of dye pollutants II. Adsorption and degradation kinetics of eosin in TiO_2 dispersions under visible light irradiation, Appl. Catal., B, 15 (1998) 147-156.

[51] R. Ocampo-Perez, C.G. Aguilar-Madera, V. Díaz-Blancas, 3D modeling of overall adsorption rate of acetaminophen on activated carbon pellets, Chem. Eng. J., 321 (2017) 510-520.

[52] E. Du, Y.X. Zhang, L. Zheng, Photocatalytic degradation of dimethyl phthalate in aqueous TiO_2 suspension: a modified Langmuir–Hinshelwood model, React. Kinet. Catal. Lett.   , 97 (2009) 83-90.

[53] J.-M. Herrmann, Heterogeneous photocatalysis: fundamentals and applications to the removal of various types of aqueous pollutants, Catal. Today, 53 (1999) 115-129.

[54] Y. Wang, C. Pan, W. Chu, A.K. Vipin, L. Sun, Environmental Remediation Applications of Carbon Nanotubes and Graphene Oxide: Adsorption and Catalysis, Nanomaterials, 9 (2019) 439.

[55] J.J. Mortensen, B. Hammer, J.K. Nørskovi, A theoretical study of adsorbate–adsorbate interactions on Ru(0001), Surf. Sci., 414 (1998) 315-329.

[56] K. Chamberlain, A.A. Evans, R.H. Bromilow, 1-octanol/water partition coefficient (K_{ow}) and pK_a for ionisable pesticides measured by a pH-metric method, Pestic. Sci., 47 (1996) 265-271.

[57] W.Z. Tang, C.P. Huang, Photocatalyzed oxidation pathways of 2,4-dichlorophenol by CdS in basic and acidic aqueous solutions, Water Res., 29 (1995) 745-756.

[58] S. Tunesi, M. Anderson, Influence of chemisorption on the photodecomposition of salicylic acid and related compounds using suspended titania ceramic membranes, J. Phys. Chem., 95 (1991) 3399-3405.

[59] A. Khataee, M. Fathinia, S. Aber, Kinetic modeling of liquid phase photocatalysis on supported TiO_2 nanoparticles in a rectangular flat-plate photoreactor, Ind. Eng. Chem. Res., 49 (2010) 12358-12364.

[60] G.F. Froment, L.H. Hosten, in: J.R. Anderson, M. Boudart (Eds.), Catal. Sci. Tech., Springer-Verlag, Berlin, pp. 97–170. (1981).

[61] J.R. Anderson, M. Boudart, Catalysis: science and technology, Springer Science & Business Media2012.

[62] M. Anantha, S. Olivera, C. Hu, B. Jayanna, N. Reddy, K. Venkatesh, H. Muralidhara, R. Naidu, Comparison of the photocatalytic, adsorption and electrochemical methods for the removal of cationic dyes from aqueous solutions, Environ. Technol. Innovation, 17 (2020) 100612.

[63] H.-L. Wang, D.-Y. Zhao, W.-F. Jiang, VIS-light-induced photocatalytic degradation of methylene blue (MB) dye using PoPD/TiO_2 composite photocatalysts, Desalin. Water Treat., 51 (2013) 2826-2835.

[64] L.T.T. Tuyen, D.A. Quang, T.T.T. Toan, T.Q. Tung, T.T. Hoa, T.X. Mau, D.Q. Khieu, Synthesis of CeO_2/TiO_2 nanotubes and heterogeneous photocatalytic degradation of methylene blue, J. Environ. Chem. Eng., 6 (2018) 5999-6011.

[65] I.Y. Habib, J. Burhan, F. Jaladi, C.M. Lim, A. Usman, N. Kumara, S.C.E. Tsang, A.H. Mahadi, Effect of Cr doping in CeO_2 nanostructures on photocatalysis and H_2O_2 assisted methylene blue dye degradation, Catal. Today, 375 (2021) 506-513.

[66] B. Mandal, J. Panda, P.K. Paul, R. Sarkar, B. Tudu, $MnFe_2O_4$ decorated reduced graphene oxide heterostructures: nanophotocatalyst for methylene blue dye degradation, Vacuum, 173 (2020) 109150.

[67] J. Tang, Z. Zou, J. Ye, Kinetics of MB degradation and effect of pH on the photocatalytic activity of MIn_2O_4 (M= Ca, Sr, Ba) under visible light irradiation, Res. Chem. Intermed., 31 (2005) 513-519.

[68] J. Matos, J. Ocares-Riquelme, P.S. Poon, R. Montaña, X. García, K. Campos, J.C. Hernández-Garrido, M.M. Titirici, C-doped anatase TiO_2: Adsorption kinetics and photocatalytic degradation of methylene blue and phenol, and correlations with DFT estimations, J. Colloid Interface Sci., 547 (2019) 14-29.

[69] P.M. Heynderickx, J.W. Thybaut, H. Poelman, D. Poelman, G.B. Marin, The total oxidation of propane over supported Cu and Ce oxides: A comparison of single and binary metal oxides, J. Catal., 272 (2010) 109-120.

[70] S. Chaemchuen, P.M. Heynderickx, F. Verpoort, Kinetic modeling of oleic acid esterification with UiO-66: from intrinsic experimental data to kinetics via elementary reaction steps, Appl. Catal. A-Gen., 394 (2020) 124816.

[71] S. Brosillon, L. Lhomme, C. Vallet, A. Bouzaza, D. Wolbert, Gas phase photocatalysis and liquid phase photocatalysis: Interdependence and influence of substrate concentration and photon flow on degradation reaction kinetics, Appl. Catal., B, 78 (2008) 232-241.

[72] M. Islam, J.B. Islam, M. Furukawa, I. Tateishi, H. Katsumata, S. Kaneco, Photocatalytic degradation of a systemic herbicide: picloram from aqueous solution using titanium oxide (TiO_2) under sunlight, ChemEngineering, 4 (2020) 58.

[73] K. Hubenko, S. Yefimova, T. Tkacheva, P. Maksimchuk, I. Borovoy, V. Klochkov, N. Kavok, O. Opolonin, Y. Malyukin, Reactive oxygen species generation in aqueous solutions containing GdVO$_4$:Eu^{3+} nanoparticles and their complexes with methylene blue, Nanoscale Res. Lett., 13 (2018) 100.

[74] F. Wang, Y. Feng, P. Chen, Y. Wang, Y. Su, Q. Zhang, Y. Zeng, Z. Xie, H. Liu, Y. Liu, W. Lv, G. Liu, Photocatalytic degradation of fluoroquinolone antibiotics using ordered mesoporous g-C$_3$N$_4$ under simulated sunlight irradiation: Kinetics, mechanism, and antibacterial activity elimination, Appl. Catal., B, 227 (2018) 114-122.

[75] C.G. da Silva, J.L.s. Faria, Photochemical and photocatalytic degradation of an azo dye in aqueous solution by UV irradiation, J. Photochem. Photobiol., A   155 (2003) 133-143.

[76] D. Ollis, C.G. Silva, J. Faria, Simultaneous photochemical and photocatalyzed liquid phase reactions: Dye decolorization kinetics, Catal. Today, 240 (2015) 80-85.

[77] N. Raza, W. Raza, H. Gul, M. Azam, J. Lee, K. Vikrant, K.-H. Kim, Solar-light-active silver phosphate/titanium dioxide/silica heterostructures for photocatalytic removal of organic dye, J. Cleaner Prod., 254 (2020) 120031.

Table 1: Experimental conditions. All experiments 1-10 are performed in duplicate and the error bars are shown in corresponding graphs. V = 25 mL for all experiments.

Experiment	Contribution in model	TBZ (mg/L)	POPs (mg/L)	q = POPs/thiabendazole	Initial pH	Light intensity (W/m^2)	Aeration
1	1, 2, 3, final	10	40	4	6.8	120	No
2	1, 2, 3, final	15	40	2.66	6.8	120	No
3	1, 2, 3, final	10	80	8	6.8	120	No
4	1, 2, 3, final	15	80	5.33	6.8	120	No
5	2, final	10	40	4	6.8	85	No
6	2, final	10	40	4	6.8	53	No
7	2, final	10	40	4	6.8	28	No
8	3, final	10	80	8	9.0	120	No
9	3, final	10	80	8	4.8	120	No
10	3, final	10	80	8	3.3	120	No
11	[a]	10	40	4	6.8	120	Yes
12	[a]	10	80	8	9.0	120	Yes
13	[a]	10	80	8	3.3	120	Yes
14	[b]	10	40	4	4.8, 6.8, 9.0	10-125	No
15	[c]	5	40	4	6.8	120	No

[a] Aeration experiments; [b] natural sunlight experiment; [c] reusability experiment.

Table 2 Estimated model parameters.

Parameter (unit)	Eq. No	Model 1	Model 2	Model 3	Final model
k_1 (g.mol^{-1} min^{-1})	(1)-(2)	$1.95\ 10^2$	$1.95\ 10^2$		
k_2 (g.L^{-1} min^{-1})	(1)-(2)	$4.22\ 10^{-4}$	$4.22\ 10^{-4}$		
$k_{1,0}$ (g.mol^{-1} min^{-1})	(16)-(17)			$1.08\ 10^2$	$1.08\ 10^2$
$k_{1,1}$ (g.mol^{-1} min^{-1})	(16)-(17)			$2.21\ 10^2$	$2.21\ 10^2$
$k_{1,2}$ (g.mol^{-1}.min^{-1})	(16)-(17)			$1.10\ 10^2$	$1.10\ 10^2$
$k_{2,0}$ (g.L^{-1} min^{-1})	(16)-(17)			$5.06\ 10^{-3}$	$5.06\ 10^{-3}$
$k_{2,1}$ (g.L^{-1} min^{-1})	(16)-(17)			$4.12\ 10^{-4}$	$4.12\ 10^{-4}$
$k_{2,2}$ (g.L^{-1}.min^{-1})	(16)-(17)			$4.93\ 10^{-3}$	$4.93\ 10^{-3}$
k_3 (min^{-1})	(1)	$4.23\ 10^{-3}$			
k_4 (min^{-1})	(2)	$1.32\ 10^{-3}$			
$k_{3,1}$ (min^{-1})	(7) or (16)		$4.23\ 10^{-3}$ (LI 120)	$4.16\ 10^{-3}$ (pH 6.8)	
$k_{3,2}$ (min^{-1})	(7) or (16)		$2.50\ 10^{-3}$ (LI 85)	$4.38\ 10^{-3}$ (pH 9)	
$k_{3,3}$ (min^{-1})	(7) or (16)		$2.19\ 10^{-3}$ (LI 53)	$2.65\ 10^{-3}$ (pH 4.8)	
$k_{3,4}$ (min^{-1})	(7) or (16)		$1.22\ 10^{-3}$ (LI 28)	$8.14\ 10^{-4}$ (pH 3.3)	
$k_{4,1}$ (min^{-1})	(8) or (17)		$1.32\ 10^{-3}$ (LI 120)	$1.68\ 10^{-3}$ (pH 6.8)	
$k_{4,2}$ (min^{-1})	(8) or (17)		$1.27\ 10^{-3}$ (LI 85)	$4.21\ 10^{-4}$ (pH 9)	
$k_{4,3}$ (min^{-1})	(8) or (17)		$4.56\ 10^{-4}$ (LI 53)	$5.30\ 10^{-3}$ (pH 4.8)	
$k_{4,4}$ (min^{-1})	(8) or (17)		$5.55\ 10^{-5}$ (LI 28)	$6.33\ 10^{-3}$ (pH 3.3)	
a	(24)				$3.45\ 10^{-7}$
b	(24)				$8.71\ 10^{-3}$
c	(25)				$6.49\ 10^{-5}$
d	(25)				$7.07\ 10^{-3}$
C_{tot} (mol g^{-1})	(3) or (18)	$8.73\ 10^{-4}$	$8.73\ 10^{-4}$	$8.73\ 10^{-4}$	$8.73\ 10^{-4}$
m	(3) or (18)	1.24	1.24	1.24	1.24
pKa_1	(11)-(13)			5.09	5.09
pKa_2	(11)-(13)			7.96	7.96
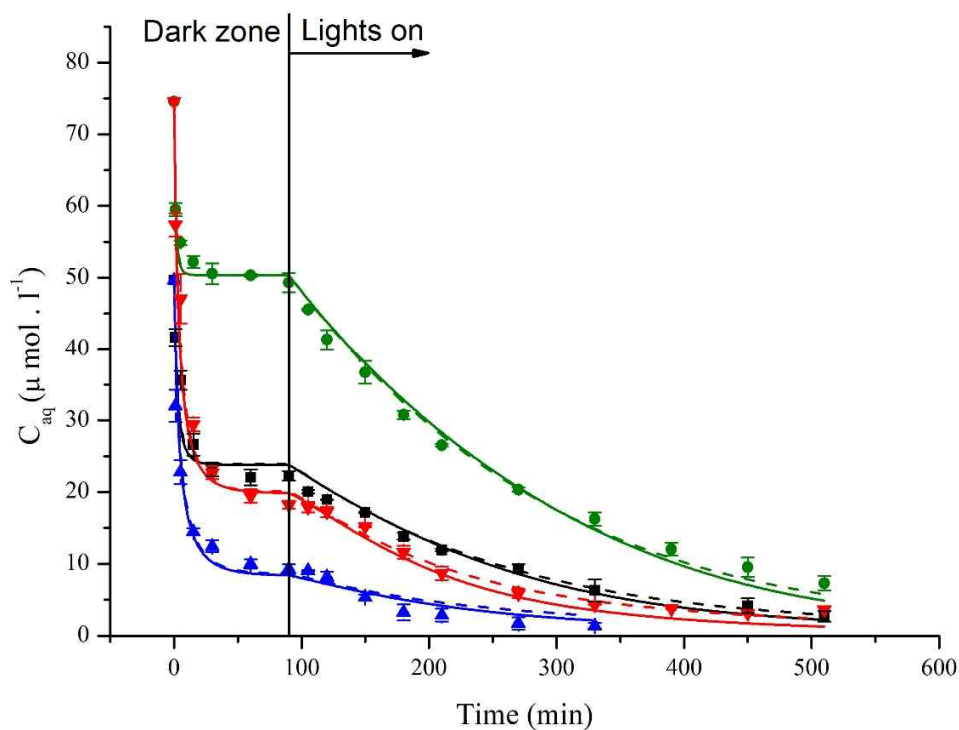
Figure 1. Effect of the POPs/TBZ ratio (q) on the measured TBZ concentration as a function of time at LI 120 W/m^2 and pH 6.8: (■) TBZ 10 mg/L & POPs 40 mg/L, (▲) TBZ 10 mg/L & POPs 80 mg/L, (▼) TBZ 15 mg/L & POPs 80 mg/L, (●) TBZ 15 mg/L & POPs 40 mg/L (experiments 1 to 4 in Table 1). Dashed lines correspond to model 1 calculated values by integration of Eqs. (1) to (3), while full lines illustrate the calculated data with the final model by integration of Eqs. (16) to (18) and k$_3$ and k$_4$ calculated by Eqs. (24) and (25).
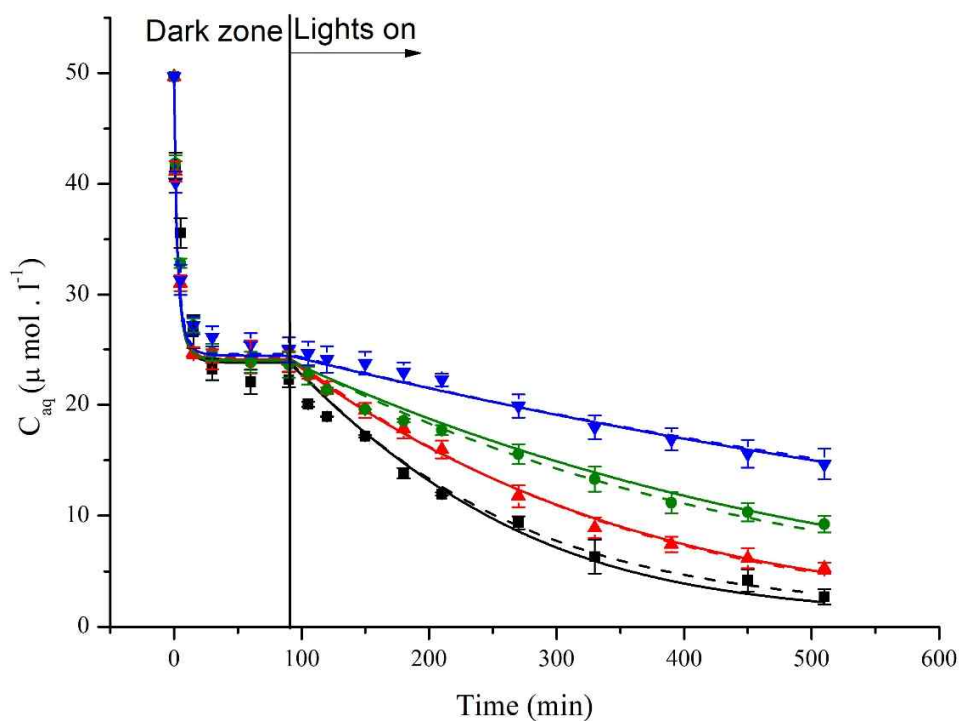
Figure 2. Effect of light intensity on the experimental TBZ concentration versus time at TBZ 10 mg/L, POPs 40 mg/L and pH 6.8: (▼) LI 28 W/m^2, (●) LI 53 W/m^2, (▲) LI 85 W/m^2, (■) LI 120 W/m^2 (experiments 1, 5, 6, and 7 in Table 1). Dashed lines correspond to model 2 calculated values by integration of Eqs. (1) to (3) and individual k_3 and k_4 mentioned in Table 2 for each light intensity. Full lines illustrate the calculated data with final model by integration of Eqs. (16) to (18) and k_3 and k_4 calculated by Eqs (24) and (25).
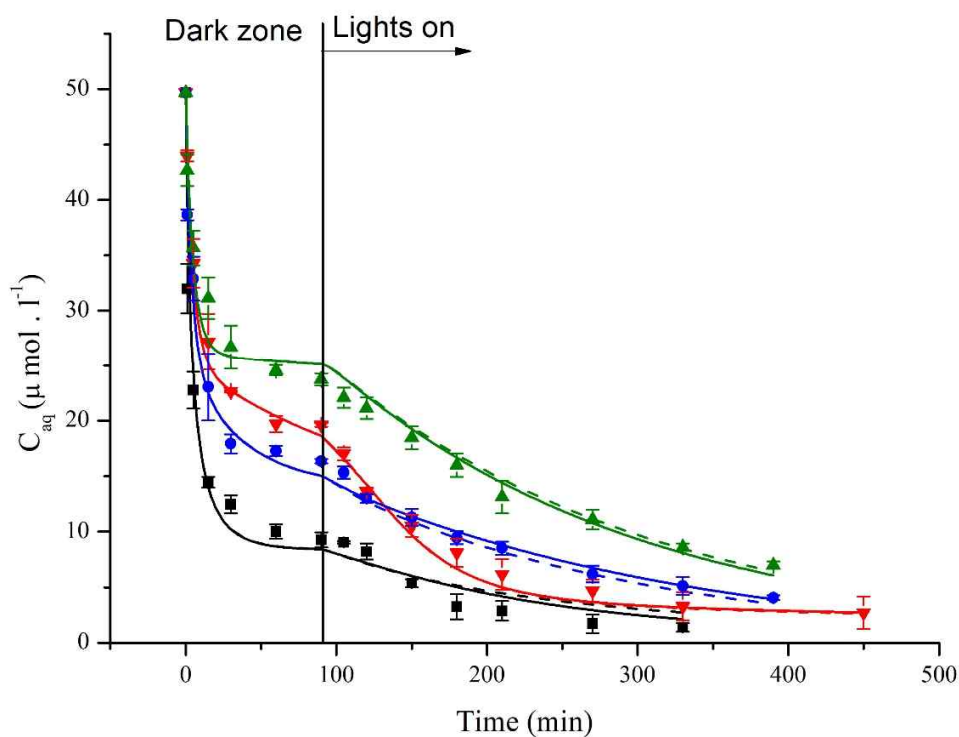
Figure 3. Effect of pH on the experimental TBZ concentration versus time at TBZ 10 mg/L , POPs 80 mg/L and LI 120 W/m^2: (▲) pH 3.3, (●) pH 4.8, (■) pH 6.8, (▼) pH 9.0 (experiments 3, 8, 9, and 10 in Table 1). Dashed lines correspond to model 3 calculated values by integration of Eqs. (16) to (18) and individual k_3 and k_4 mentioned in Table 2 for each pH. Full lines illustrate the calculated data with final model by integration of Eqs. (16) to (18), and k_3 and k_4 calculated by Eqs. (24) and (25).
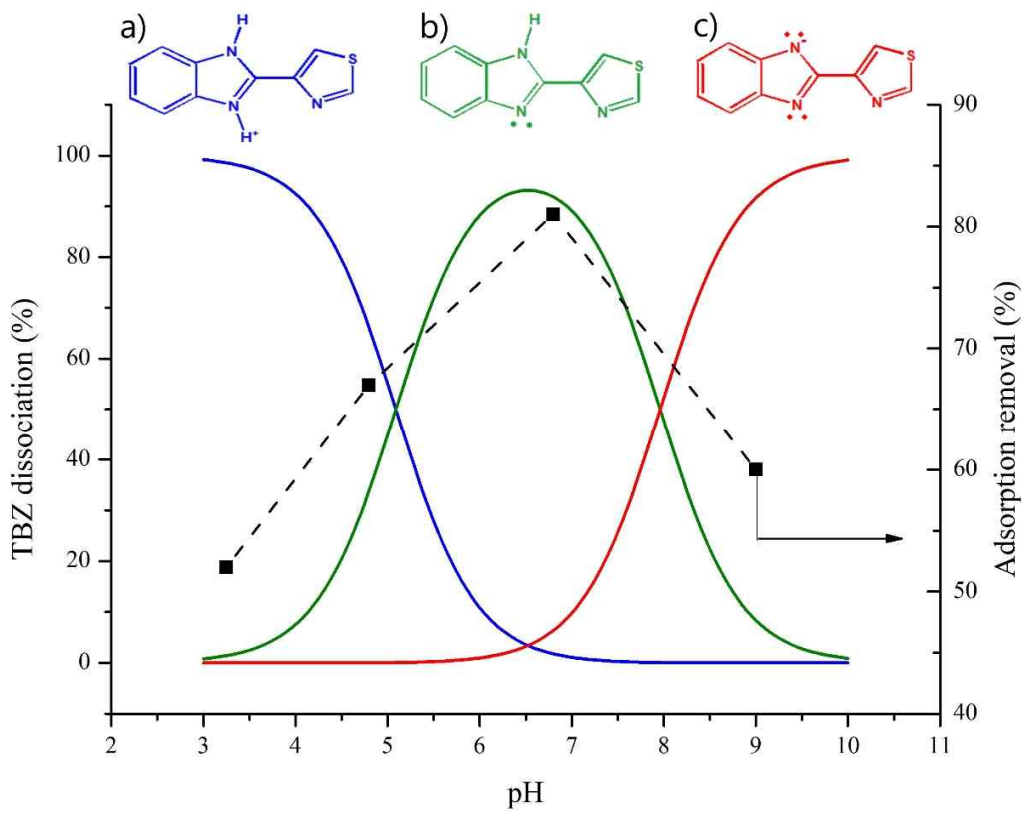
Figure 4. TBZ speciation and liquid phase removal by adsorption as a function of pH. Full lines are calculated by Eqs. (11) to (13) having $pKa_1 = 5.09$ and $pKa_2 = 7.96$: (a) positive specimen (—) $[AH_2^+]$, (b) neutral specimen (—) $[AH]$, (c) negative specimen (—) $[A^-]$, (■) TBZ removal (%) in the dark phase. TBZ 10 mg/L, POPs 80 mg/L, LI 120 W/m^2 (experiments 3, 8, 9, and 10 in Table 1).
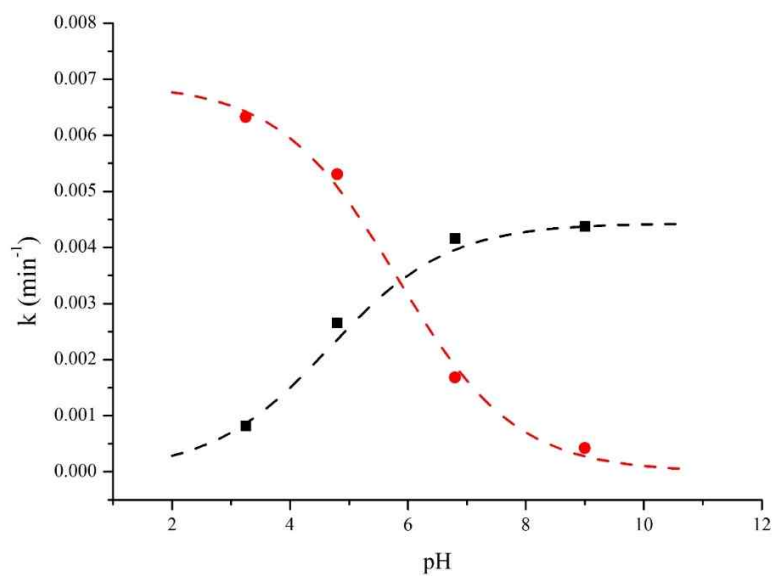
Figure 5. Individual k_3 (■) and k_4 (●) at different pH values, calculated by model 3 via integration of Eqs. (16) to (18). (- - -) k_3 trend line Eq. (24), (- - -) k_4 trend line Eq. (25). TBZ 10 mg/L, POPs 80 mg/L, LI 120 W/m^2 (experiments 3, 8, 9, and 10 in Table 1).
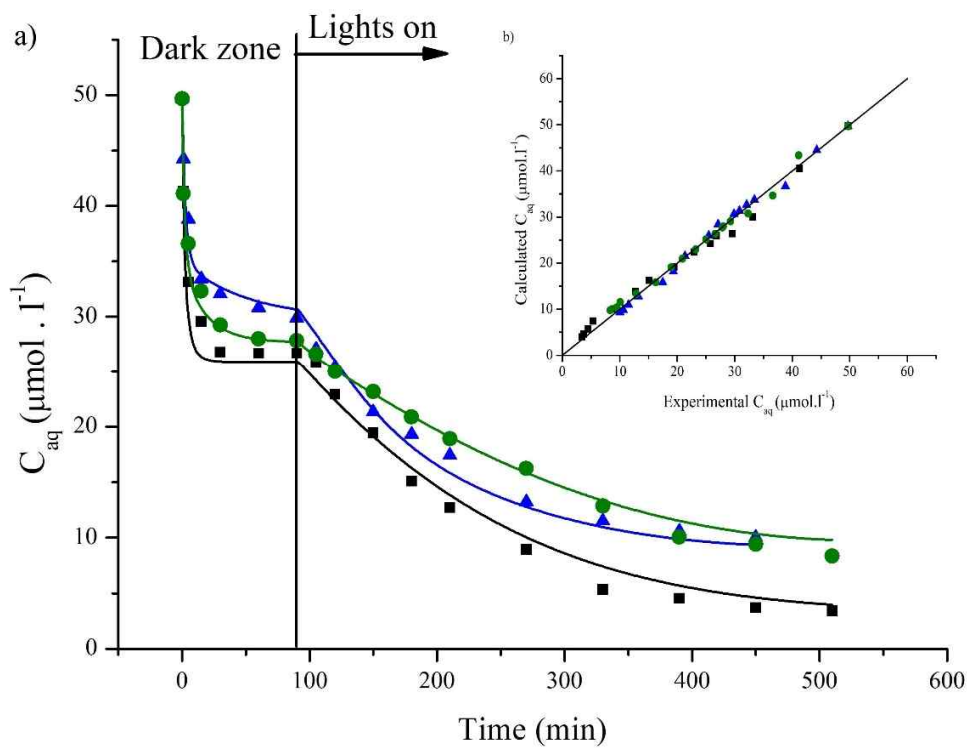
Figure 6. Model validation experiments (TBZ 10 mg/L, POPs 40 mg/L) under natural sunlight at (■) pH 6.8, (●) pH 4.8, (▲) pH 9. Full lines illustrate the calculated data with the final model by integration of Eqs. (16) to (18) and k_3 and k_4 calculated by Eqs. (24) and (25). b) Parity plot of experimental versus calculated data of the model validation experiments. TBZ 10 mg/L, POPs 40 mg/L.
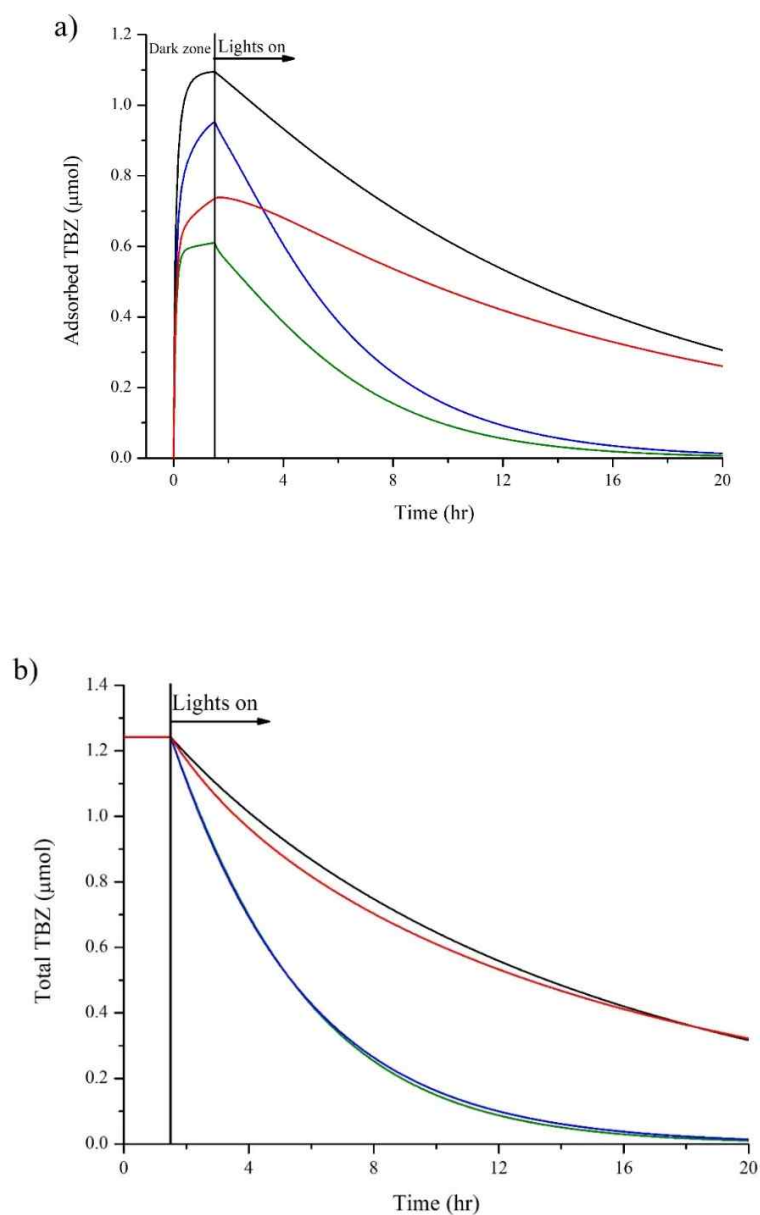
Figure 7. a) Simulated total amount of adsorbed TBZ molecules on the catalyst surface versus time calculated by Eq. (17), b) Simulated total amount of unreacted TBZ molecules in the process, calculated by Eq. (31). (—) pH 3.3, (—) pH 4.8, (—) pH 6.8, (—) pH 9.0; TBZ 10 mg/L, POPs 80 mg/L, LI 120 W/m^2.
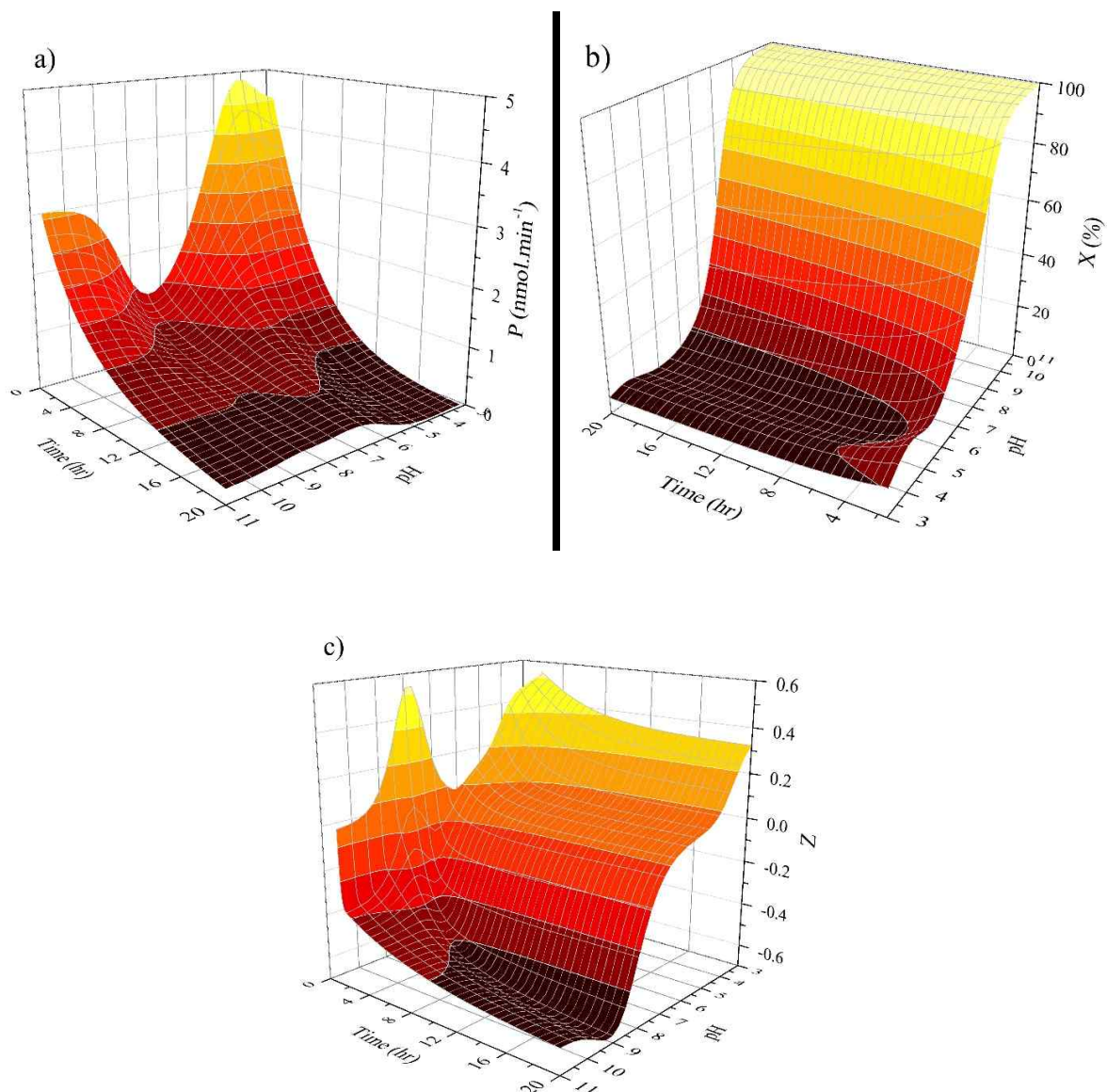
Figure 8. a) Total TBZ degradation rate (P) calculated by Eq. (32) as a function of pH and time, b) Ratio of the aqueous TBZ degradation over its total degradation (X) calculated by Eq. (33) as a function of pH and time, c) Ratio of the TBZ total adsorption over its total degradation (Z) calculated by Eq. (34) as a function of pH and time. TBZ 10 mg/L, POPs 80 mg/L, LI 120 W/m^2.
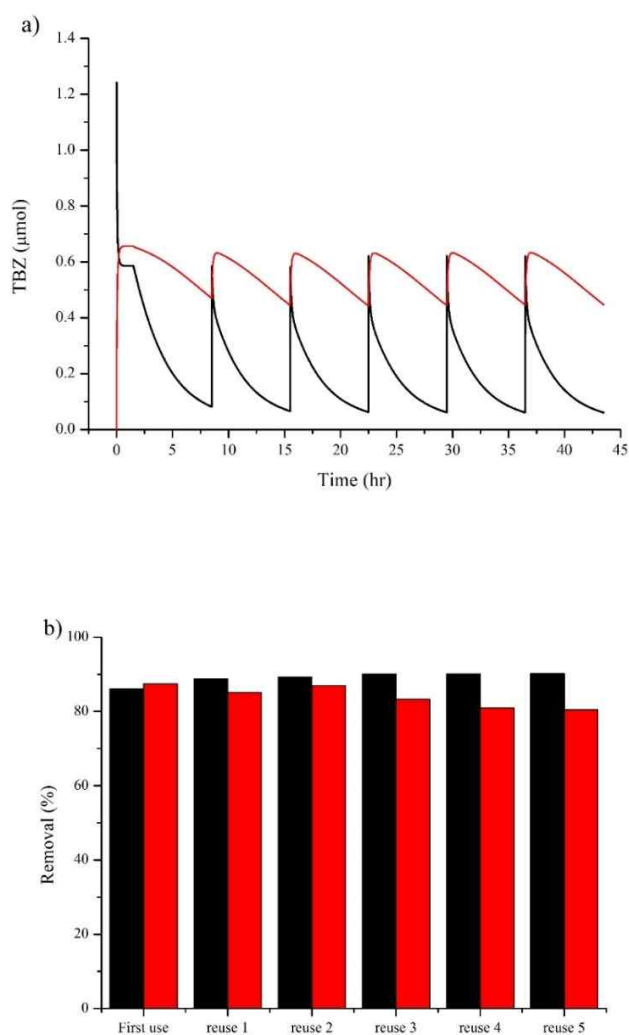
Figure 9. Simulated and experimental data of photocatalytic TBZ degradation on POPs. a) Simulation of total moles of (—) aqueous and (—) adsorbed TBZ as a function of time. b) (■) simulated and (■) experimental TBZ removal from the solution. Initial TBZ concentration 10 mg/L and aqueous TBZ concentration at the beginning of each reuse cycle 5 mg/L, LI 120 W/m², POPs 40 mg/L, pH 6.8.